Research Square

Preprints are preliminary reports that have not undergone peer review.
They should not be considered conclusive, used to inform clinical practice,
or referenced by the media as validated information.

# Ionotropic Gelation Synthesis of Berberine Loaded Alginate Nanoparticles with Physicochemical Characterization and Multifunctional Biological Activities

**Mohadeseh Arabhalvaei**
Semnan University of Medical Sciences
**Marjan Bahraminasab**
m82bahraminasab@gmail.com

Semnan University of Medical Sciences
**Zahra Nazemi**
Semnan University
**Samaneh Arab**
Semnan University of Medical Sciences
**Akram Alizadeh**
Semnan University of Medical Sciences
**Mohammad Sadegh Nourbakhsh**
Semnan University

**Research Article**

**Keywords:** Berberine, Sodium alginate, Drug delivery system, Nanoparticles, Anticancer, Anti-inflammatory

**Posted Date:** September 10th, 2026

**DOI:** https://doi.org/10.21203/rs.3.rs-10478927/v1

**License:** This work is licensed under a Creative Commons Attribution 4.0 International License.
Read Full License

**Additional Declarations:** No competing interests reported.

# Ionotropic Gelation Synthesis of Berberine Loaded Alginate Nanoparticles with Physicochemical Characterization and Multifunctional Biological Activities

Mohadeseh Arabhalvaei [1], Marjan Bahraminasab [2,3*], Zahra Nazemi [4], Samaneh Arab [2,5], Akram Alizadeh [2,3], Mohammad Sadegh Nourbakhsh [4]

[1] Student Research Committee, Semnan University of Medical Sciences, Semnan, Iran

[2] Department of Tissue Engineering and Applied Cell Sciences, School of Medicine, Semnan University of Medical Sciences, Semnan, Iran

[3] Nervous System Stem Cells Research Center, Neuroscience Research Institute, Semnan University of Medical Sciences, Semnan, Iran

[4] Faculty of New Sciences and Technologies, Semnan University, Semnan, Iran

[5] Cancer Research Center, Semnan University of Medical Sciences, Semnan, Iran

∗Corresponding authors: Marjan Bahraminasab

E-mail addresses: m82bahraminasab@gmail.com, Tel: +989102861236, Semnan University of Medical Sciences, Bassij Blvd, Semnan, Iran. Postal Code: 35147-99442

## Abstract

**Background and Aim:** Nanoparticle (NP)- formulated drug delivery platforms can enhance therapeutic efficacy and bioavailability while reducing limitations such as poor drug solubility and systemic side effects. This study focuses on the synthesis and characterization of berberine (BBR)-loaded sodium alginate (SA) NPs and evaluates their biological activities as a controlled drug delivery platform.

**Methods:** BBR-loaded SA NPs were prepared and characterized for particle size, zeta potential, morphology, FTIR profile, entrapment efficiency, loading capacity, and drug release. Cytotoxicity was assessed in MC3T3-E1 pre-osteoblast cells, and cellular uptake was examined by FE-SEM. Osteogenic differentiation was evaluated using alkaline phosphatase (ALP) and alizarin red assays. Anti-inflammatory, anticancer, and antibacterial activities were also investigated.

**Results:** FTIR confirmed successful BBR incorporation into SA NPs. These NPs had a size of 183.9 ± 74.17 nm by FE-SEM, zeta potential of -21.47±0.25 mV, entrapment efficiency of 91.8±0.4%, and loading capacity of 19.6±0.1%. A sustained release profile of ~10% over 14 days was observed, along with cellular uptake. The formulation exhibited no observable cytotoxicity at 1.25–2560 µg/mL (viability of > 70%). At 640 µg/mL, the NPs caused the highest ALP activity, mineralization, and cancer cell death. The concentration of 640 µg/mL showed the greatest increase in ALP activity, mineralization, and cancer cell death. The concentrations of 640 and 1280 µg/mL showed anti-inflammatory effect. Antibacterial activity was slight and moderate, respectively, against *Pseudomonas aeruginosa* (< 20%) and *Staphylococcus aureus* (< 60%).

**Conclusion:** BBR-loaded SA NPs showed biocompatibility, sustained release, osteogenic potential, and promising anti-inflammatory and anticancer activities.

**Keywords:** Berberine, Sodium alginate, Drug delivery system, Nanoparticles, Anticancer, Anti-inflammatory

## 1. Introduction

Berberine (BBR) is a naturally derived isoquinoline alkaloid isolated from several medicinal plants, including Berberis vulgaris, which possesses potent medicinal properties such as antimicrobial, anti-inflammatory, antioxidant, antidiabetic, anticancer and hepatoprotective effects (1, 2). BBR exerts anti-inflammatory effects through regulation of major signaling pathways such as NF-κB (Nuclear Factor kappa B) and MAPK (Mitogen-Activated Protein Kinase), thereby reducing the expression of pro-inflammatory cytokines (3, 4). Moreover, it has shown promise in inhibiting the proliferation of tumor cells, stimulating apoptosis, and suppressing metastasis progression in several cancer models (5, 6). Recent studies have also highlighted its potential benefits in bone tissue applications, including the promotion of osteoblastic differentiation and the inhibition of osteoclast activity, suggesting its promise for the treatment of bone-related inflammatory diseases and bone cancers such as osteosarcoma (7-11).

Despite these favorable properties, the pharmacokinetics of BBR have certain restrictions. For instance, its low absorption through the intestinal wall results in low bioavailability, following oral administration. Furthermore, oral intake of BBR may lead to intestinal side effects, such as cramps, stomach upset, and alterations in intestinal microbiota (12). Additionally, the intravenous administration of BBR results in limited and variable distribution, while the formation of aggregates hampers its cellular uptake (13). Consequently, the drug is rapidly cleared, and its bioavailability remains inadequate. Furthermore, BBR has deprived aqueous solubility, which severely limits its clinical application and necessitates the development of advanced delivery systems to enhance its pharmacokinetic profile. Therefore, a delivery system for BBR should surmount the obstacles of solubility, further enhance its effectiveness, and minimize accumulation in native tissues to prevent undesired adverse effects (14).

Drug delivery using nanoparticles (NPs) has been developed and studied for many years with the aim of enhancing the availability and effectiveness of pharmaceutical agents (15-18). Drug nanocarriers offer numerous advantages compared to administering free drugs. These include protection against drug degradation, prolonged circulation time in the body, enhanced bioavailability of hydrophobic drugs, and controlled drug release (19). Moreover, nanocarriers enable maximizing

therapeutic outcomes of many drugs by providing influential dose at damaged sites (20). These valuable drug carriers can be composed of various materials depending on their intended applications and requirements. Among them, polymeric NPs have been widely attracted attention in delivery of different drug formulations via various roots of administrations (21). Non-covalent interactions within polymeric matrices allow stable incorporation of hydrophobic drugs like BBR, thereby overcoming limitations associated with poor solubility and unfavorable systemic distribution (22, 23). Furthermore, modifications such as folic acid conjugation have been employed to improve the targeted delivery of BBR to cancer cells, demonstrating significant potential in oncology applications (24). The versatility of BBR-loaded NPs extends to numerous therapeutic areas. For instance, in the diabetes mellitus management, the antioxidant and anti-inflammatory properties of BBR have been enhanced through nanoencapsulation, leading to improved glycemic control in animal models (25). Similarly, cancer therapy has benefited from BBR-loaded NPs, with targeted delivery systems such as folic acid-modified chitosan or mesoporous silica carriers showing increased cytotoxicity against cancer cells while sparing healthy tissues (24, 26).

Both synthetic and natural polymers are of interest as BBR nanocarriers (27-29). Natural polymers have been widely studied for their biocompatibility and biodegradability. Among them, sodium alginate (SA) has been extensively investigated because of its superior physicochemical properties. This polymer is non-toxic, biocompatible, biodegradable, cost-effective, and easily accessible with non-immunogenic properties (30). SA is an anionic polymer derived from brown algae and bacteria, consisting of linearly linked α-L-guluronic acid (G) and β-D-mannuronic acid (M) residues connected by 1,4-glycosidic bonds (31, 32). SA provides several benefits for pharmaceutical and biomedical applications, including drug delivery systems, cell encapsulation and three-dimensional (3D) cell culture (33-35). This polymer offers additional advantages as a carrier, enhancing the stability and efficacy of BBR formulations (29, 33, 36). Mehra et al. (33) used the ionic gelation method to prepare SA-based NPs for BBR delivery. They evaluated nanoparticle size, morphology, and drug encapsulation efficiency and its release from NPs to confirm the formulation's potential for effective drug delivery. The developed BBR-loaded NPs showed that 76% of BBR released within 48 h at pH of 7.4 using the phosphate buffer saline (PBS) at 37 °C. Furthermore, Kumar et al. (36) also prepared chitosan-coated SA NPs loaded with BBR using the ionic gelation

technique. They applied Box–Behnken design to optimize process parameters and evaluated particle size, zeta potential, entrapment efficiency, and drug release in vitro. In a pH 7.4 PBS, an in-vitro drug release investigation on an optimized batch of Berberine HCl nanoparticles (BE-OPT) revealed around 96% release over 12 h. Moreover, Kohli et al. (29) developed natural polysaccharide-based NPs (SA and chitosan) to improve the BBR oral bioavailability. Using a green and biocompatible approach, they optimized the formulation through design of experiments and evaluated its performance through ex vivo and in vivo studies. The NPs significantly improved BBR's solubility, permeability, and absorption. The release profile showed that 75.06 ± 4.2% of BBR immersed in PBS with pH 7.4 and 0.5% v/v tween 80 dissolution media was released in 24 h. Despite the utility of these alginate-based delivery systems, it can be indicated that maintaining an optimal therapeutic window remains challenging. Therefore, controlled and sustained release is crucial for BBR delivery, as it can maintain effective drug levels for longer periods, reduce plasma concentration fluctuations, and decrease dosing frequency. In contrast, the burst release reported in the existing studies for BBR-loaded SA NPs, where much of the drug is released within a few hours, may restrict therapeutic efficacy.

Therefore, developing nanocarrier systems capable of providing a slower release of BBR in a controlled manner is essential to improve its pharmacological effectiveness and expand its clinical utility. In this study, BBR-loaded SA NPs were fabricated using the ionic gelation method following approaches reported in previous studies, but with use of a crosslinking agent and by focusing on the evaluation of the biological behaviors and a prolonged release achievement. The concentration of the crosslinking agent ($CaCl_2$) used in the present study was selected based on our previous work, in which the effect of crosslinker concentration on the particle size of SA Nps was investigated (37). While earlier investigations have mainly focused on the physicochemical characterization of these NPs, including particle size distribution, zeta potential, and encapsulation efficiency, many of the reported formulations exhibited relatively rapid BBR release profiles.

Consequently, one of the main objectives of this study was to develop SA NPs capable of providing a more controlled and sustained release of BBR in order to prolong drug availability and potentially improve its therapeutic effectiveness. The central hypothesis of the present study was that $CaCl_2$-crosslinked SA NPs could provide a sustained-release platform for BBR, particularly for bone-related inflammatory conditions, by prolonging drug availability while maintaining

cytocompatibility with normal osteoblastic cells. Accordingly, the biological assays were selected primarily to evaluate the suitability of the formulation for this intended application, while additional antibacterial and anticancer assessments were included as complementary indicators of its broader bioactivity.

## 2. Materials and method:

### 2.1. Materials

SA powder and BBR were provided from Sigma Aldrich, London. Natural honey used in this study was purchased from a well-known beekeeper in Semnan, Iran, and analytical grade calcium chloride ($CaCl_2$, Merck, Darmstadt, Germany) was used to crosslink the BBR-loaded SA NPs. All cell culture reagents, including Dulbecco's Modified Eagle Medium (DMEM), fetal bovine serum (FBS) and penicillin–streptomycin, were purchased from Bio Idea Company, Iran. Furthermore, L-ascorbic acid, and β-glycerophosphate were provided from Sigma-Aldrich, USA.

### 2.2. Synthesis of BBR-loaded SA NPs

The ionotropic gelation method was utilized to synthesis SA NPs as shown in Figure 1, based on recent studies (37, 38). Initially, $CaCl_2$ powder was dissolved in distilled water to achieve a homogeneous solution (0.04% w/v). Separate solutions of BBR and SA were prepared. First, 10 mg of BBR was dissolved in 2 mL of distilled water. In parallel, 100 mg of sodium alginate was dissolved in 8 mL of distilled water containing 100 mg of honey, which was used as a stabilizing agent. Honey was included only during nanoparticle preparation to improve the stability of the dispersion and to assist in obtaining a more uniform nanoparticle system. The two solutions were then mixed to achieve 1% w/v SA, 1% w/v honey, and 0.1% w/v BBR (a ratio of 1:10 for BBR to SA). This solution was stirred thoroughly until a homogeneous final mixture was obtained. Subsequently, the $CaCl_2$ solution was added dropwise to this mixture at 1000 rpm with a rate of 1 mL/min. The beaker was then covered with aluminum foil and stirred at 1000 rpm for 4 hours at room temperature. The dispersion was subsequently ultrasonicated (Farasoat Iranian, Iran) at 100 Wat for 2 hours, and centrifuged (Universal 320R) at 6000 rpm for 20 minutes, followed by three washing cycles with distilled water to remove residual free BBR and honey.

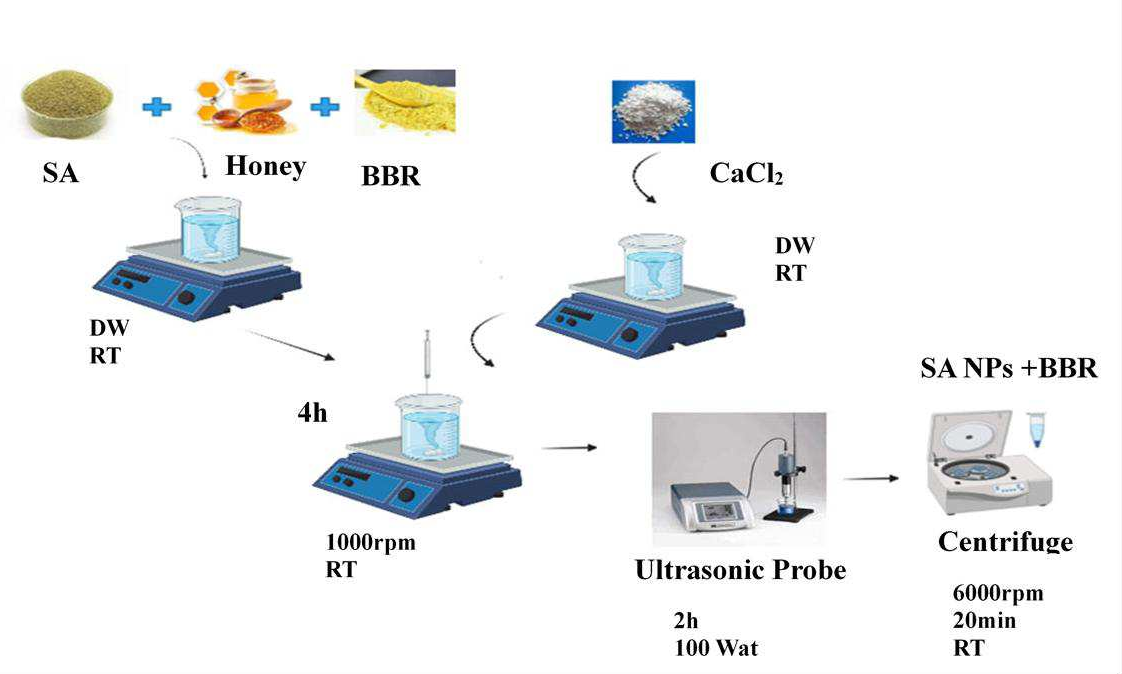



**Figure 1.** Synthesis of SA NPs containing BBR (DW: distilled water, RT: room temperature, BBR: berberine, SA: sodium alginate)

## 2.3. Nanoparticle characterizations

Particle size, with and without BBR, was determined using the dynamic light scattering (DLS) method using Horiba Company, SZ100. Zeta potential was measured to indicate the NPs surface charge. Moreover, field emission scanning electron microscopy (FE-SEM, Sigma 300-HV, Zeiss, Germany) was used to analyze the SA NPs morphology and size distribution. The chemical bonding characteristics in the synthesized NPs were examined by Fourier transform infrared spectroscopy (FTIR, Thermo, Avatar, USA).

## 2.4. Entrapment efficiency, drug loading and yield

To evaluate BBR encapsulation in SA NPs, the absorbance of the post-centrifugation supernatant (after NPs recovery) was measured at 421 nm (λmax) using a microplate reader (Synergy H1 Hybrid Multi-Mode Microplate Reader, Bio Tek Company, USA). Absorbance readings were converted to BBR concentrations using a standard calibration curve. The amount of unencapsulated BBR was taken as the drug concentration in the supernatant, and the entrapped fraction was calculated as the

difference between the initial BBR input and the free BBR remaining in solution. Entrapment efficiency (EE%) was then determined using Eq. 1.

$$EE\ (\%) = \frac{Wa - Wb}{Wa} \times 100 \qquad (1)$$

where *Wa* is the initial mass of drug added and *Wb* is the mass of unencapsulated (free) drug. In addition, the drug loading capacity (LC%) was estimated using Eq. 2.

$$LC\ (\%) = \frac{\mathrm{W_D}}{W_{N+D}} \times 100 \qquad (2)$$

where $W_D$ denotes the mass of the encapsulated drug and $W_{N+D}$ represents the mass of the dried drug-loaded nanoparticles. BBR-loaded NPs were freeze-dried and weighed to determine drug loading.

The yield of NPs was calculated by measuring the weight of dry SA NPs without drug ($W_N$), and the weight of initial SA ($W_{SA}$) used for their synthesis, using equation 3. SA NPs without drug were freeze-dried, and the dry weight was recorded to determine the yield.

$$\text{Yeild}_{\,SA\ NPs}(\%) = \frac{\mathrm{W_N}}{W_{SA}} \times 100 \qquad (3)$$

Yield of NPs containing BBR was calculated by measuring the weight of dry drug-containing NPs ($W_{N+D}$), the weight of initial SA ($W_{SA}$), and the weight of initial drug ($W_D$), using equation 4.

$$\text{Yeild}_{\,SA+D\ NPs}(\%) = \frac{W_{N+D}}{W_D + W_{SA}} \times 100 \qquad (4)$$

**2.5. Drug release**

For the release study, 4 mL of a deionized-water suspension of BBR-loaded SA NPs was placed into a dialysis bag and sealed. The bag was then immersed in 40 mL of deionized water and incubated at 37 °C with continuous stirring (200 rpm) for 15 days. At predetermined intervals (1, 3, 6, 24, 48, and 72 h, and subsequently up to day 15), 1 mL aliquots were collected from the external medium and immediately replaced with an equal volume of fresh deionized water. The absorbance of the collected samples was measured at 421 nm using a spectrophotometer (Synergy H1

Hybrid Multi-Mode Microplate Reader, BioTek, USA). The cumulative release of BBR was then calculated based on a previously established standard curve in deionized water.

### 2.6. Biological tests

#### 2.6.1. Cell culture

MC3T3-E1 (Subclone 4 mouse preosteoblasts) and MG-63 (human osteosarcoma cell line) cells were purchased from Sigma Aldrich, Sweden and the Iranian Biological Resource Center, respectively. The cells were maintained at 37 °C in a humidified incubator (95% humidity, 5% $CO_2$) in DMEM supplemented with 10% FBS and 100 U/mL penicillin–streptomycin.

#### 2.6.2. Cytocompatibility on normal bone cells

The Alamar Blue assay (a resazurin-based membrane permeable solution, Sigma Aldrich, London) was used to assess the metabolic activity of MC3T3-E1 cells. A total of $5\times10^{3}$ cells were seeded in 96-well plates and allowed to attach for 24 hours, after which they were exposed to various concentrations of BBR, SA NPs, and BBR-loaded SA NPs (N+B) ranging from 1.25 µg/mL to 2560 µg/mL. The plates were incubated for 1 and 3 days at 37 °C. After incubation, Alamar Blue reagent was then added to the wells, and the plates were incubated for an additional 4 hours at 37 °C in a 5% $CO_2$ atmosphere. Next, 100 µL of each well supernatant was transferred to a black 96-well plate, and fluorescence absorbance was quantified by means of a microplate reader (Synergy H1 Hybrid Multi-Mode Microplate Reader, BioTek, USA) at an excitation wavelength of 570 nm and an emission wavelength of 600 nm.

#### 2.6.3. Differentiation toward bone cells

The higher doses of BBR-loaded SA NPs were chosen for cell differentiation based on the previously reported data (39, 40).

##### 2.6.3.1. Alkaline phosphatase activity

$2 \times 10^{3}$ MC3T3-E1 cells/well of 96-well plates were seeded and cultured for 24 hours, followed by exposing to BBR-loaded NPs (N+B) at concentrations ranging from 640 µg/mL to 2560 µg/mL. To induce osteogenic differentiation, the culture medium was supplemented with L-ascorbic acid (50 µg/mL) and β-

glycerophosphate (10 mM). On days 7 and 14, alkaline phosphatase (ALP) concentration was evaluated using the SensoLyte pNPP ALP Colorimetric Assay Kit (AnaSpec Inc., USA). For the assay, cell lysates were prepared using Triton X-100 (100 µL/well) and incubated with the chromogenic ALP substrate (pNPP) at ambient temperature for 20 minutes. Absorbance was measured at 405 nm, and enzyme concentration was quantified using a standard curve generated from serial dilutions of calf intestine ALP (100 to 0 ng/mL).

#### 2.6.3.2. Alizarin red assay for mineralization

As an indicator of calcium deposition, alizarin red staining performed after 7 days of culture. MC3T3-E1 cells ($5 \times 10^3$ per well of a 48-well plate) were cultured in an incubator at 37 °C with $CO_2$ and 95 % humidity for 24 hours to allow formation of a monolayer. The cells were then treated with various concentrations of BBR-loaded NPs (N+B) ranging from 640 µg/mL to 2560 µg/mL, while osteogenic supplements containing L-ascorbic acid (50 µg/mL), and β-glycerophosphate (10 mM) were concurrently added. At day 7, cells were fixed with paraformaldehyde (4 v/v%) for 15 min at 4 °C, washed with PBS, and stained with alizarin red (1 w/v %) for 40 min at room temperature in the dark. Excess dye was removed by repeated PBS washes, and the plates were photographed.

### 2.6.4. Anti-inflammation activity

To evaluate the anti-inflammatory effects of BBR-loaded NPs, MC3T3-E1 cells ($2\times10^4$ cells per well) were seeded into 24-well plates. Then, $1.5\times10^4$ *Staphylococcus aureus* (ATCC 25923) colony-forming units (CFU)/mL were added to induce an inflammatory response. The cells were subsequently exposed to different concentrations of NPs (640, 1280, and 2560 µg/mL) and incubated for 24 hours at 37 °C with 5% $CO_2$. The higher doses were chosen here based on the previous studies, which have identified their effectiveness for anti-inflammatory effect (41, 42). After treatment, the culture supernatants were collected and centrifuged to remove debris. The pro-inflammatory cytokines levels, including TNF-α and IL-6, were quantified using enzyme-linked immunosorbent assay (ELISA) kits (BioLegend, San Diego, CA, USA) according to the manufacturer's protocols. Cytokine concentrations were determined based on standard curves, and the results were analyzed to assess the anti-inflammatory activity of the NPs.

### 2.6.5. Cytotoxicity in cancer cells

The cytotoxicity and anti-proliferative effects of BBR-loaded SA NPs were evaluated using the Alamar Blue assay (Sigma Aldrich, London). MG63 cells were plated in 96-well culture plates at a seeding density of $5 \times 10^3$ cells/well and incubated for 24 hours. The MG63 cells were subsequently exposed to various concentrations of NPs (640, 1280, and 2560 µg/mL). The higher concentrations were chosen based on the previous studies (43). After 1, 3, and 7 days of incubation, Alamar Blue reagent was added to the wells, and the plates were further incubated for 4 hours at 37 °C in a 5% $CO_2$ atmosphere. Subsequently, 100 µL of each well supernatant was transferred to black 96-well plates, and the fluorescence intensity was recorded using a microplate reader at an excitation wavelength of 570 nm and an emission wavelength of 600 nm.

### 2.6.6. Cellular uptake assessment

MC3T3-E1 cells ($2 \times 10^3$ cells per well) were seeded on a coverslip and exposed to 20 µg/mL of BBR-loaded NPs (N+B). These were incubated at 37 °C in a humidified atmosphere with 5% $CO_2$ for 24 hours. After incubation, the medium was aspirated, and the cells were washed with PBS. The cells were then fixed with 4 v/v% paraformaldehyde at 4 °C, followed by air-drying at room temperature for 30 min. The cellular uptake was subsequently examined using FE-SEM (MIRA3 TESCAN-XMU, Czech Republic).

## 2.7. Antibacterial activity

### 2.7.1. Bacteria strains and growth

The strains of *Staphylococcus aureus* (ATCC 25923) and *Pseudomonas aeruginosa* (ATCC 27853) were cultured in nutrient broth (Ibresco,Iran) at 37℃ and 200 rpm. After reaching an optical density of 0.5 at 600 nm, corresponding to the beginning of the exponential growth phase or ~$1.5 \times 10^8$ CFU /mL, the bacteria were harvested on the day of the infection experiments.

### 2.7.2. Minimum inhibition concentration (MIC) assay

The MIC of BBR against *Staphylococcus aureus* and *Pseudomonas aeruginosa* was identified using the broth microdilution method in sterile 96-well plates, following CLSI guidelines with minor modifications (44). Two-fold serial dilutions were

prepared in liquid Broth (LB, Ibresco, Iran) to achieve final concentrations ranging from 2560 µg/mL to 1.25 µg/mL. Each well received 50 µL of the respective BBR dilution. This was also done for SA NPs and BBR-loaded SA NPs. The turbidity of the bacteria suspensions was initially adjusted to correspond to the 0.5 McFarland standard (~$1.5 \times 10^8$ CFU/mL), then diluted 1:1000 in LB to obtain a final inoculum of $1.5 \times 10^5$ CFU/mL. Subsequently, 10 µL of the bacterial suspension was added to each well containing the BBR dilutions, and 40 µL of LB was added to each well, bringing the final volume in each well to 100 µL. Control wells included bacteria with LB (no BBR) as the positive control ($C^+$) and LB only (no bacteria) as the negative control ($C^-$). The plates were incubated overnight at 37 °C, after which the optical density at 600 nm ($OD_{600}$) was recorded using a microplate reader (Synergy H1 Hybrid Multi-Mode Microplate Reader, BioTek, USA). The bacteria growth inhibition percentage was estimated using equation 5. The MIC was determined as the lowest tested concentration that fully prevented visible bacterial growth.

$$\text{Inhibition (\%)} = \frac{OD\ C^+ - OD\ sample}{OD\ C^+} \times 100 \qquad (5)$$

### 2.7.3. Minimum bactericidal concentration (MBC) analysis

MBC is the lowest concentration of an antimicrobial agent that produces a 3-log reduction, corresponding to 99.9% killing, in the initial inoculum of a standard bacterial strain. The MBC test serves as a complement to the MIC test. To determine the MBC, 50 µL aliquots from the dilution selected as the MIC and at least two more concentrated dilutions were plated onto Mueller-Hinton Agar (MHA) and incubated at 37 °C for 24 hours. Following incubation, the plates were examined for bacterial colony formation.

### 2.8. Statistical analysis

Data were analyzed using one-way or two-way ANOVA in Minitab (v17). Differences were considered statistically significant at $\alpha = 0.05$ (95% confidence level).

## 3. Results

### 3.1. Nanoparticle characterization

#### 3.1.1. Particle size

The DLS-Zeta analysis showed that the average particle size of the drug-free NPs (Figure 2a) was 193.87 ± 4.61 nm, and the average zeta potential (Figure 2b) was –2.27 ± 0.56 mV. For the BBR-loaded NPs, the average particle size was 432.27 ± 11.67 nm, and the average zeta potential was –21.47 ± 0.25 mV. As it was expected, the particle size increased due to the encapsulation of BBR within the NPs. Further to the increase in particle size, a marked change in zeta potential was observed after BBR encapsulation.

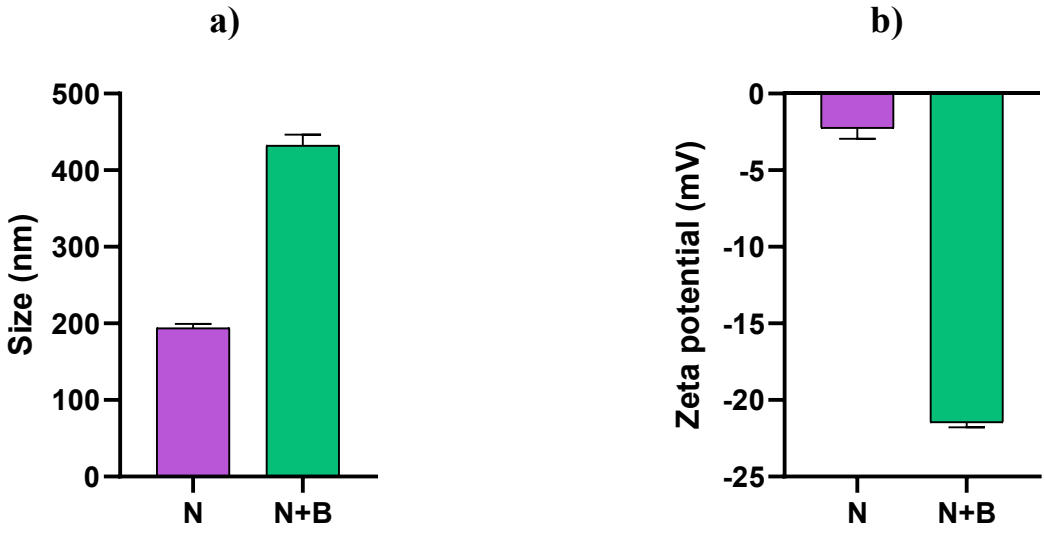



**Figure 2.** a) Size, and b) Zeta potential of SA NPs without BBR (N) and with BBR (N+B)

The morphology and particle size distribution of SA NPs without and with BBR were also determined by FE-SEM and ImageJ software, as shown in Figures 3a and 3b, respectively. FE-SEM findings revealed that the nanoparticle morphology remained consistent after drug loading; the particles were predominantly spherical, with a small fraction exhibiting irregular shapes. The average particle size of SA NPs without BBR was 103.8 ± 47.27 nm (Figure 3a). FE-SEM micrograph of SA NPs with BBR is presented in Figure 3b. Their morphology closely resembled that of SA NPs without BBR. The average particle size of SA NPs containing BBR was 183.9 ± 74.17 nm (Figure 3b). In contrast, sizes reported via DLS were larger, likely attributable to the hydrated layer around the particles in suspension and their

tendency to aggregate during DLS analysis, as well as particle fusion in SEM imaging.

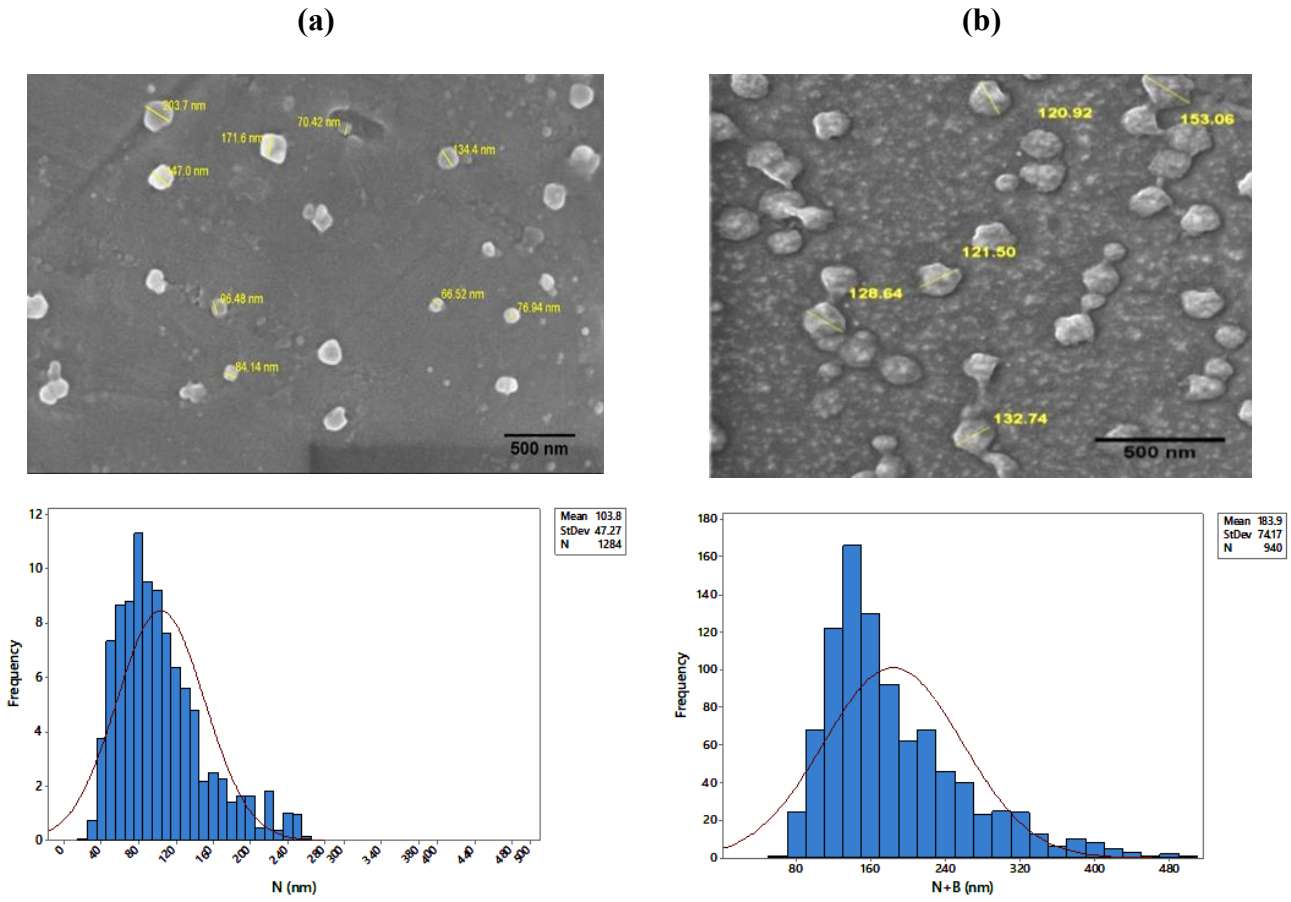



**Figure 3.** FE-SEM micrographs and size dispersion of SA NPs; a) without BBR (N), and b) with BBR (N+B)

### 3.1.2. Chemical bonds

The FTIR spectrum of BBR (Figure 4) exhibits characteristic peak in the range of 3550-3200 $cm^{-1}$, possibly corresponding to O–H and N–H stretching vibrations (45, 46). The peak at 3055 $cm^{-1}$ is attributed to C–H stretching in aromatic groups, while peaks at 2908 $cm^{-1}$ and 2846 $cm^{-1}$ indicate alkane C–H stretching (47). The peaks at 1605 $cm^{-1}$ and 1637 $cm^{-1}$ are assigned to C=C stretching within the aromatic ring and an iminium double bond ($C=N^{+}$), respectively (48). The characteristic bands at 1396 $cm^{-1}$ and 1365.60 $cm^{-1}$ are associated with C–H bending, whereas the peaks at

1293.02 $cm^{-1}$ and 1204.44 $cm^{-1}$ indicate the existence of C–O and C–N bonds, particularly in cyclic amine structures (49). The bands at 825 $cm^{-1}$, 640 $cm^{-1}$, 524 $cm^{-1}$, 424 $cm^{-1}$, and 393 $cm^{-1}$ (bellow 900 $cm^{-1}$) suggest the presence of out-of-plane C–H bending in aromatic structures (47). The FTIR spectrum of SA NPs, shown in Figure 4, exhibits a broad peak around 3430 $cm^{-1}$, attributed to hydrogen-bonded O–H stretching (50). Peaks at 1631 $cm^{-1}$ and 1403 $cm^{-1}$ are associated with the asymmetric and symmetric stretching of carboxylate ($COO^-$) groups, in respect (50). The region between 1100 and 1000 $cm^{-1}$ shows characteristic bands associated with C–O–C stretching in the alginate backbone (51) .

As shown in Figure 4, the FTIR spectrum of the BBR-loaded NPs displayed similar peaks to those of pure BBR, confirming the effective drug incorporation into the nanoparticle structure. Carboxylate groups ($COO^-$), the asymmetric band, shift from 1631 $cm^{-1}$ (SA) to 1610 $cm^{-1}$ (SA NPs + BBR) with a decrease in intensity. The symmetric band shift from 1403 $cm^{-1}$ (SA NPs) to 1410 $cm^{-1}$ (SA NPs + BBR), also with a slight decrease in intensity. The O–H band shifts from 3430 $cm^{-1}$ (SA NPs) to 3270 $cm^{-1}$ (SA NPs + BBR) with increased intensity.

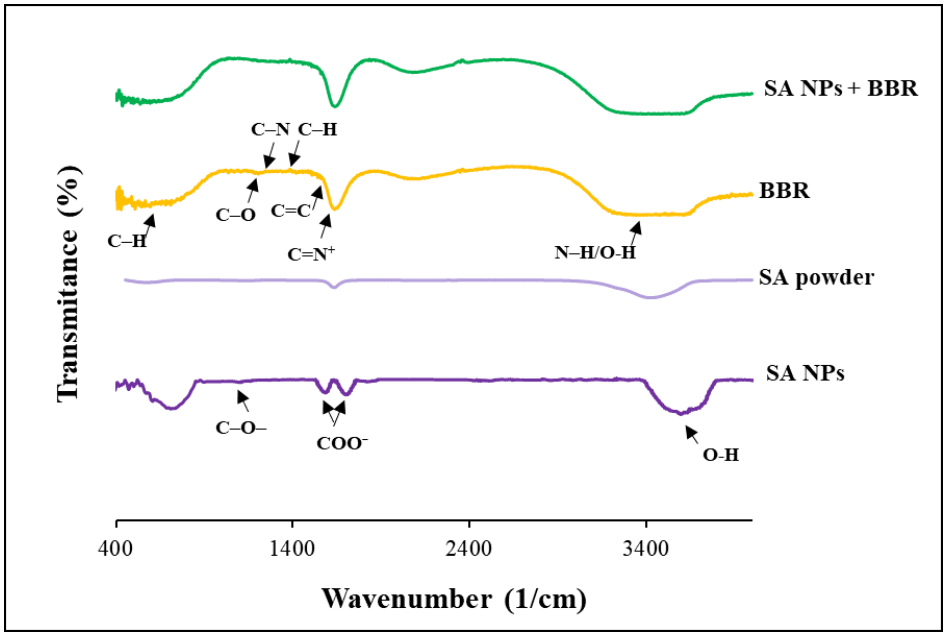



**Figure 4.** FTIR spectra of BBR, SA powder, and SA NPs with BBR and without BBR.

## 3.2. Entrapment efficiency, drug loading and yield

The percentages of entrapment efficiency and loading capacity were identified. EE % and LC % of the BBR-loaded NPs were found to be 91.82 ± 0.48% and

19.66 ± 0.10%, respectively. These results demonstrate that the encapsulation process was highly effective, achieving excellent drug incorporation within the nanoparticles. The high EE% suggests minimal drug loss during formulation, while the LC% reflects the potential for effective therapeutic delivery with reduced carrier burden (52). The production yield of NPs was evaluated both in the presence and absence of BBR. NPs without BBR exhibited a yield of 46.7 ± 0.008%, while BBR-loaded NPs showed a lower yield of 30.27 ± 0.0003%.

### 3.3. Drug release profile

The results showed that SA NPs containing BBR released approximately 3% of the encapsulated drug over the initial 6 hours (Figure 5a). On 336 hours (14 days), around 10% of the BBR was released from the NPs (Figure 5b). SA NPs containing BBR exhibited a slow and sustained release profile, which is advantageous for maintaining effective drug levels over extended periods. This release behavior can reduce dosing frequency and limit peak-related side effects, thereby improving therapeutic efficiency. Moreover, the prolonged release is particularly beneficial for localized applications, as it may enhance drug availability at the target site while minimizing systemic exposure.

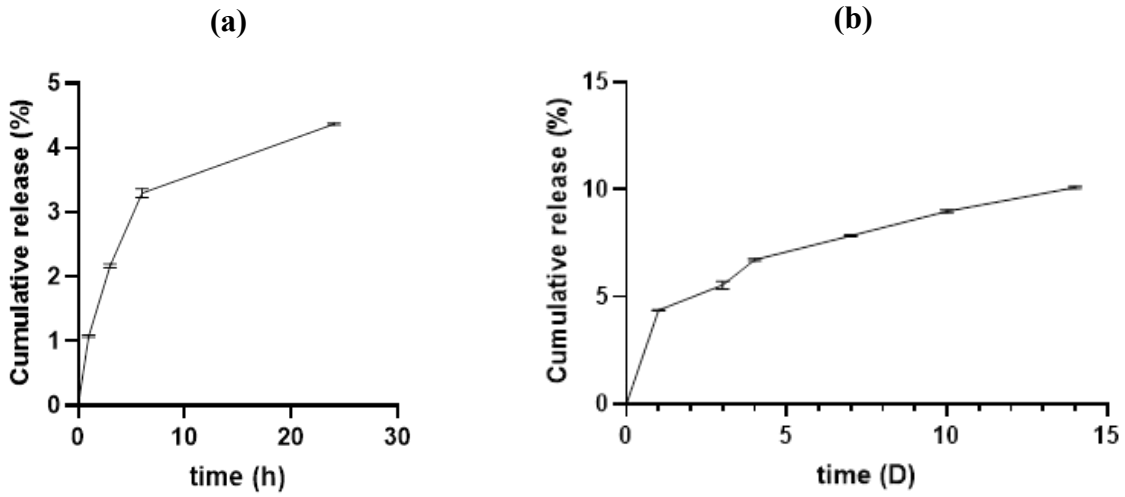



**Figure 5.** Drug release from SA NPs containing BBR; a) The first 24 hours, and b) total release until day 15

### 3.4. Biological evaluations

#### 3.4.1. Osteoblast cell viability

Alamar Blue test was used to measure the viability of MC3T3-E1 cells (normal pre-osteoblasts) over 1- and 3-day exposure periods to free BBR, and NPs without and with BBR (identified as B, N, and N+B, respectively, in Figure 6). As it is shown, survival remains above 70% at all concentrations, and NPs alone, free drug, and NPs containing BBR show no toxicity to normal osteoblastic cells.

Across all three experimental groups, cell viability exhibited a clear dose- and time-dependent pattern. In the BBR group (B), viability peaked at B1.25 (98.5%) and dropped to its minimum at B2560 (75.6%) on day 1. B1.25 and B160 revealed the highest (99.2%) and lowest (78.0%) viability on day 3, respectively. In the nanoparticle group (N), the highest viability was recorded at the lowest concentration (N1.25) on day 1, and the lowest viability occurred at N320 on day 3. In the BBR-loaded nanoparticle group (N+B), the maximum viability appeared at N+B1.25 on day 1 (103.8%), while the lowest value was detected at N+B640 on day 3 (75,5%).

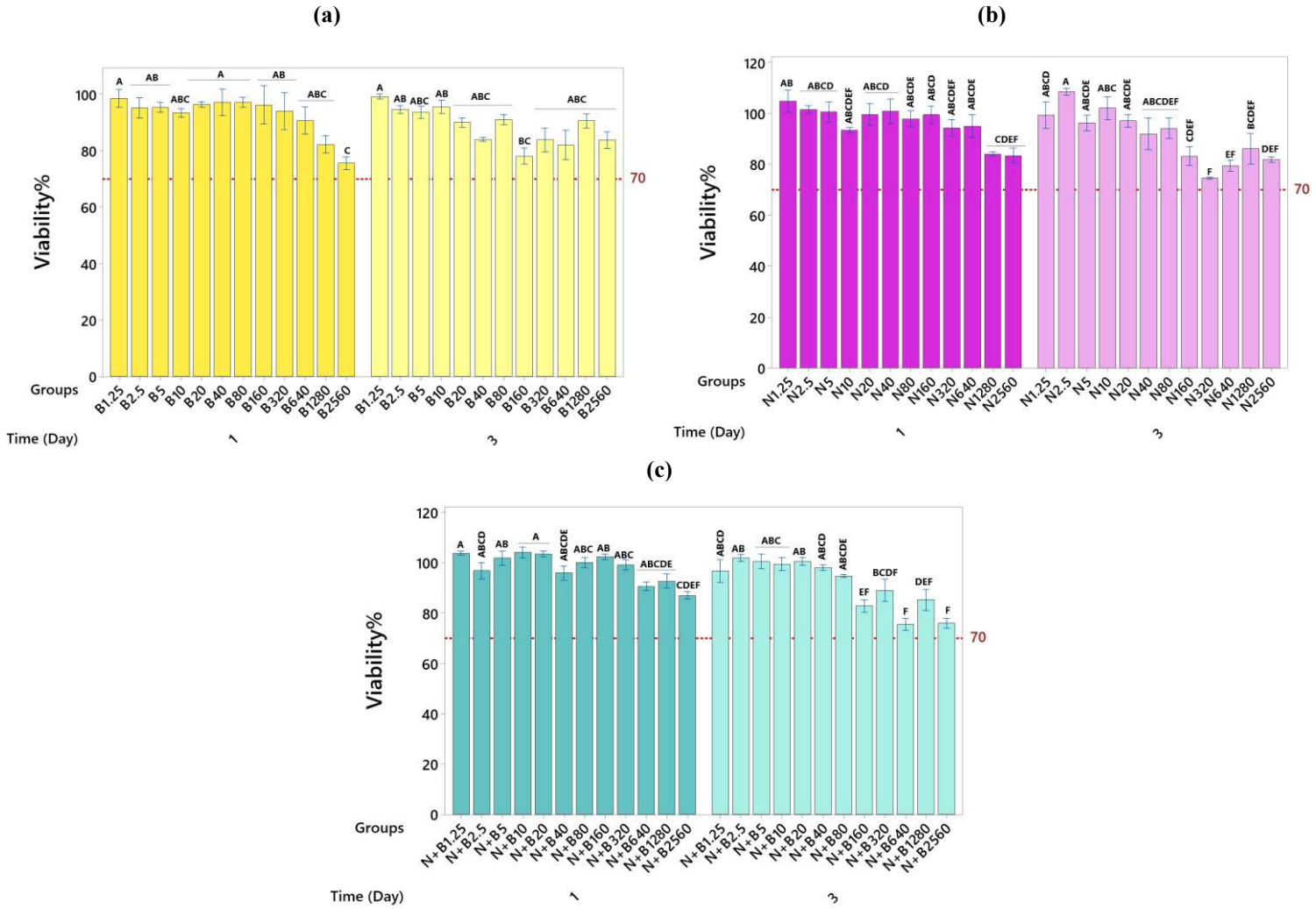



**Figure 6.** Alamar Blue results on MC3T3-E1 cells treated with (a) free BBR, (b) blank SA NPs, and (c) BBR loaded SA NPs (B, N and N+B, respectively). Groups not sharing the same letter differ significantly ($p < 0.05$).

### 3.4.2. Osteoblastic differentiation and mineralization

An alkaline phosphatase assay was accomplished to assess the differentiation of MC3T3-E1 cells at 7 and 14 days. The 640 µg/mL concentration of BBR-containing NPs enhanced the rate of osteogenic differentiation relative to the control at both 7 and 14 days. The increase was significant compared to the control at day 7 (Figure 7a). On day 7, ALP levels increased progressively from the control (7.3 ng/mL) to N+B 2560 µg/mL (8.4 ng/mL), while on day 14, the levels were lower and more uniform across all groups, ranging from 6.6 ng/mL in the control to 6.7 ng/mL in N+B 2560.

Alizarin Red staining, as a measure of calcium deposition, was measured at day 7 on MC3T3-E1 cells. As shown in Figure 7b, the 640 µg/mL concentration of BBR-containing NPs showed the highest osteogenic differentiation rate. Alizarin Red stain specifically binds to calcium ions, forming a stable orange-red complex that reflects the degree of extracellular matrix mineralization. Thus, the intensity of red staining directly indicates the level of calcium deposition and the progression of osteogenic differentiation. In our study, all BBR-loaded SA nanoparticle treatment groups showed stronger Alizarin Red stain intensity than control, confirming enhanced mineralization. Notably, the 640 µg/mL group (N+B640) exhibited the most pronounced staining, indicating that this concentration was the most effective in promoting calcium deposition, rather than the highest tested dose. This pattern aligns well with our ALP results, where the N+B640 group also showed the greatest increase in ALP activity, which is an established early marker of osteogenesis (Figure 7). The consistency between ALP activity and Alizarin Red staining supports the conclusion that the nanoparticle formulation enhances osteogenic differentiation, with 640 µg/mL identified as the optimal dose.

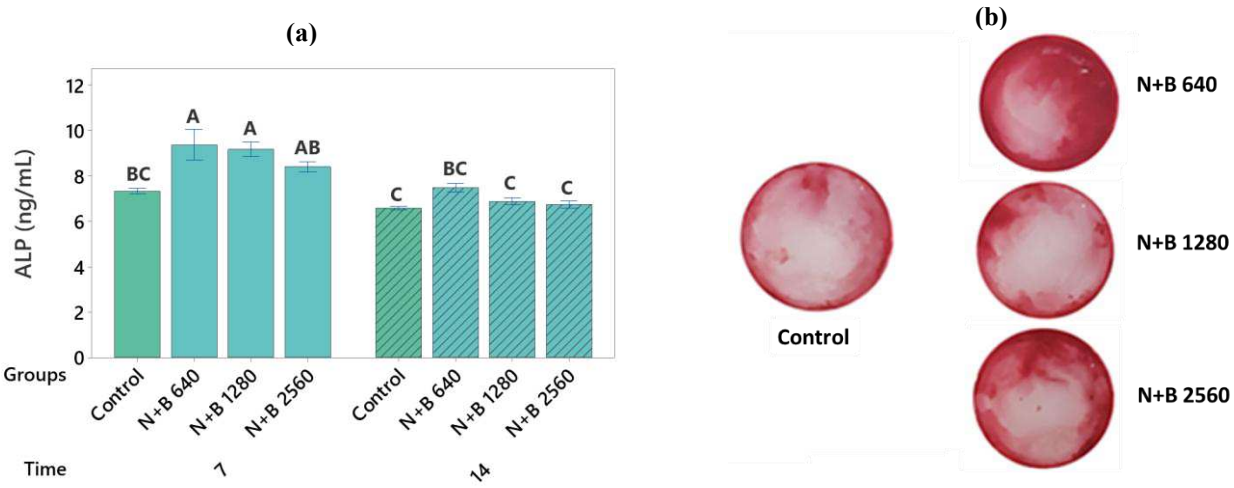



**Figure 7.** a) ALP and b) Alizarine red staining results on MC3T3-E1 cells at different concentrations of BBR-loaded SA NPs (N+B). Mean values that do not share a common letter are significantly different ($p < 0.05$).

### 3.4.3. Inflammation factors

The levels of pro-inflammatory cytokines (TNF-α and IL-6) are shown in Figure 8, which reveals a reduction in IL-6 cytokine concentration in all groups compared with the control (Cell+Bacteria, no treatment). The most pronounced reduction in the inflammatory response occurred at a concentration of 640 µg/mL (N+B640). Specifically, the IL-6 concentration decreased from approximately 39 pg/mL in the control group to 24.2 pg/mL at 640 µg/mL, corresponding to an estimated ~38% reduction. This trend indicates a notable suppressive effect of the NPs at lower concentrations on IL-6 secretion. Similarly, for TNF-α, all treatments decreased the TNF-α secretion with highest reduction caused by N+B1280 (15.6 pg/mL) followed by N+B640 (17.3 pg/mL) compared to the control group (30.9 pg/mL).

Despite these observable trends and the apparent anti-inflammatory potential, no statistically significant differences were detected among the groups for IL-6 ($p > 0.05$). However, the reduction in TNF-α secretion was statistically significant at 1280 µg/mL (N+B1280).

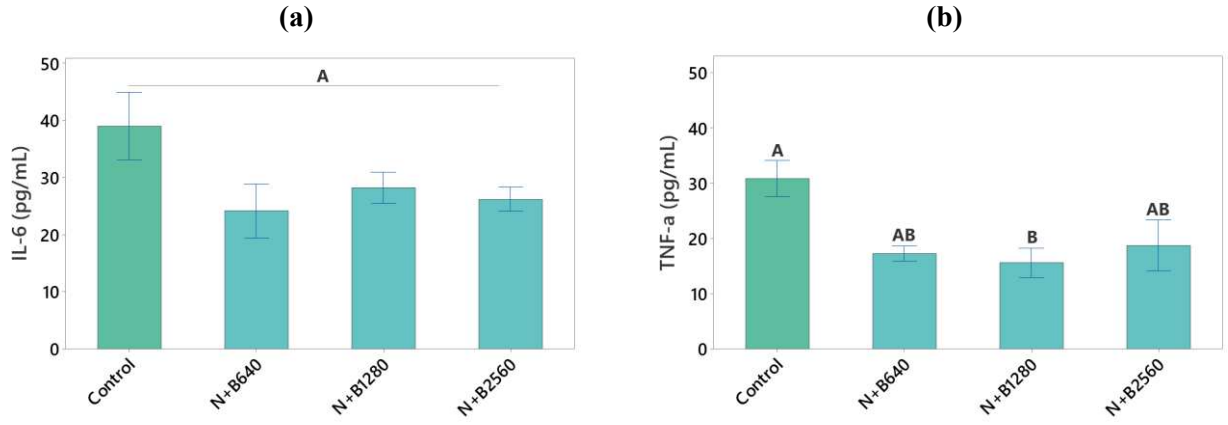



**Figure 8.** Inflammatory cytokine concentrations in the culture medium of MC3T3-E1 cells at different concentrations of SA NPs with BBR (N+B); (a) IL-6, and (b) TNF-α. Groups not sharing the same letter differ significantly ($p < 0.05$).

### 3.4.4. Cytotoxicity in cancer cells

The cytotoxicity and anti-proliferative effects of various concentrations of BBR-loaded SA NPs on MG63 cells were evaluated using the Alamar Blue assay (Figure 9). The NPs containing 640 µg/mL concentration of BBR caused more toxicity on

MG63 cells (cell viability rates at 1, 3, and 7 days were 73.97 %, 67.47 %, and 42.25 %, respectively) than the 1280 µg/mL (90.04 %, 80.22 %, and 65.84 %) and 2560 µg/mL (104.9 %, 81.49 % and 99.99) concentrations. A significant difference was observed between the cell viability between N+B640 and the other groups at day 7. Increasing the exposure time of the cells to the NPs increased toxicity. For 2560 µg/mL, cell viability at day 3 was significantly lower than at day 1 and day 7 ($p < 0.05$), while no significant difference was between day 1 and day 7. For 1280 µg/mL, viability at day 1 was significantly higher than at day 7 ($p < 0.05$). For 640 µg/mL, the viability at day 7 was significantly inferior to those at day 1 and day 3 ($p < 0.05$), whereas no significant difference was detected between day 1 and day 3.

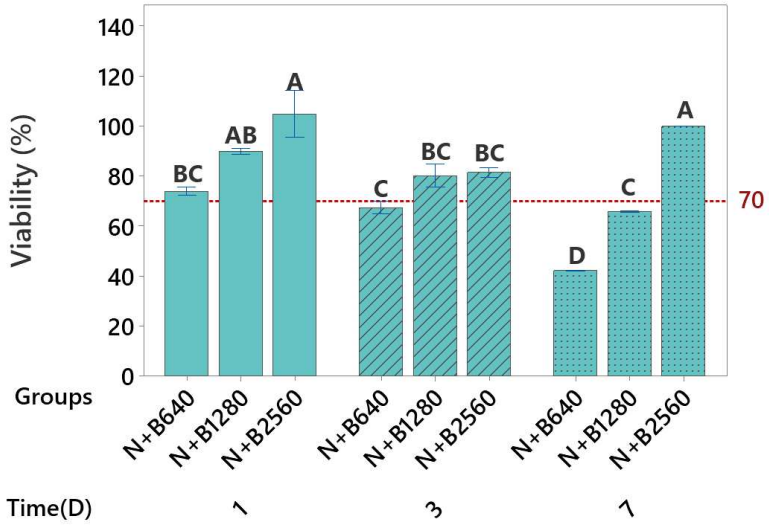



**Figure 9.** Alamar Blue results on MG63 cells at different groups of SA NPs with BBR (N+B). Mean values that do not share a common letter are significantly different ($p < 0.05$).

### 3.4.5. Cellular uptake assay

Figure 10 presents FE-SEM micrographs of MC3T3-E1 cells in the control group and those treated with BBR-loaded NPs (640 µg/mL). The images indicate that several NPs entered the cells (orange arrows). The particles were observed not only on the cell surface but also within the cytoplasmic region and, in some cases, in close to the nucleus, indicating successful internalization. Overall, the observed interaction between the BBR-loaded SA NPs and the cellular architecture supports their potential as an effective delivery system capable of achieving meaningful intracellular bioavailability. It should be noted that the NPs uptake by cellular systems generally occurs via endocytosis, and is governed by their by the

physicochemical properties characteristics, including size, shape, and surface chemistry. (53).

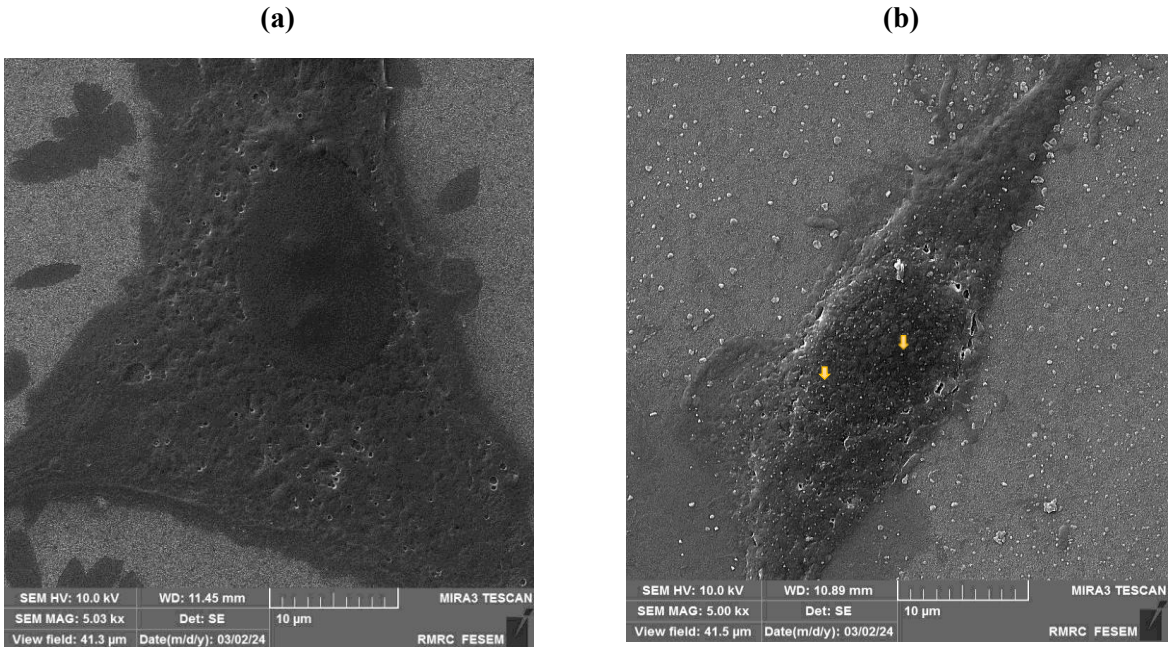



**Figure 10.** FE-SEM micrograph of MC3T3-E1 cellular uptake of NPs; a) without treatment with NPs (control group), and b) treated with BBR-loaded SA NPs.

## 3.5. Bacterial tests

### 3.5.1. Minimum inhibition concentration (MIC)

As illustrated in Figures 11, different concentrations of BBR, SA NPs with and without BBR were tested, and the MIC was determined based on the lowest dose that successfully prevented bacterial proliferation. As it can be seen in the Figure, the maximum inhibitory% for *Staphylococcus aureus* and *Pseudomonas aeruginosa* was < 60% and <25%, respectively, in all testing groups. No concentration could fully prevent bacterial growth in 24 hours. Concentrations of 5, 10, and 20 µg/mL of BBR (with 47.93%, 50.42% and 48.73% growth inhibition percentages, in respect), 40, 80, and 160 µg/mL of NPs without BBR (47.97%, 50.87% and 53.01%), and 5, 10, and 20 µg/mL of NPs with BBR (54.08%, 53.24% and 53.82%) were selected as the best doses for *Staphylococcus aureus* bacteria. The results for *Pseudomonas aeruginosa* bacteria showed that the best concentrations were considered to be 5, 10, and 20 µg/mL of BBR (15.41%, 21.88% and 11.66%), 320, 640, and 1280 µg/mL of NPs without BBR (14.59%, 18.57% and 19.77%), and 5, 10, 20 µg/mL and 40 µg/mL of NPs with BBR (16.61%, 15.07%, 12.72% and 15.79%). These concentrations

were chosen for MBC based on the differences in growth inhibition and the statistical differences and significance.

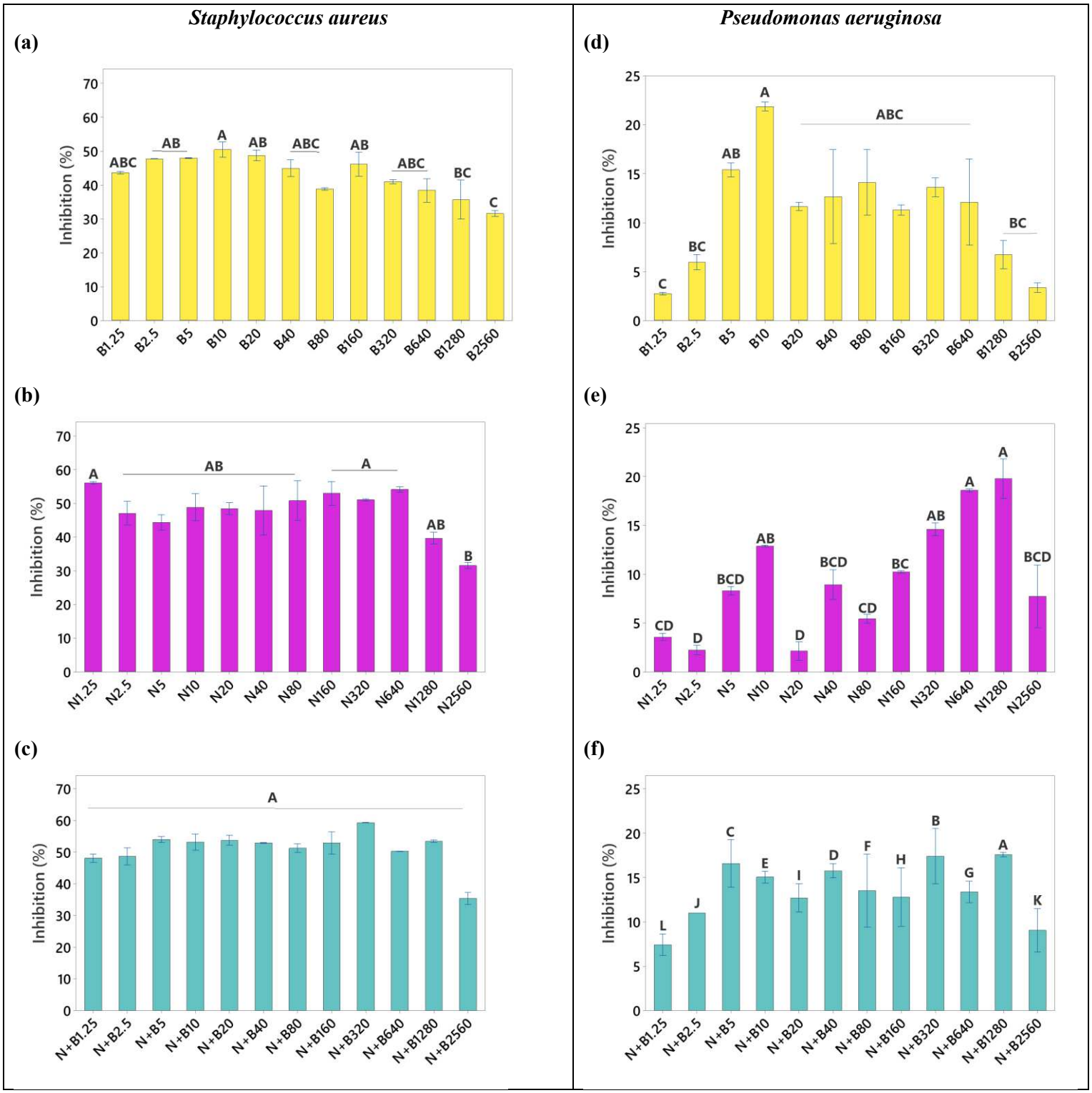



**Figure 11.** MIC on *Staphylococcus aureus* and *Pseudomonas aeruginosa* at different groups of free BBR, blank SA NPs, and BBR-loaded SA NPs (B, N and N+B, respectively)

### 3.5.2. Minimum Bactericidal Concentration (MBC)

To further evaluate the antibacterial efficacy of the NP formulations, the MBC was determined. The results are presented in Figure 12. No minimum bactericidal concentration was detected for the tested samples, suggesting that the formulations possess bacteriostatic rather than bactericidal properties.

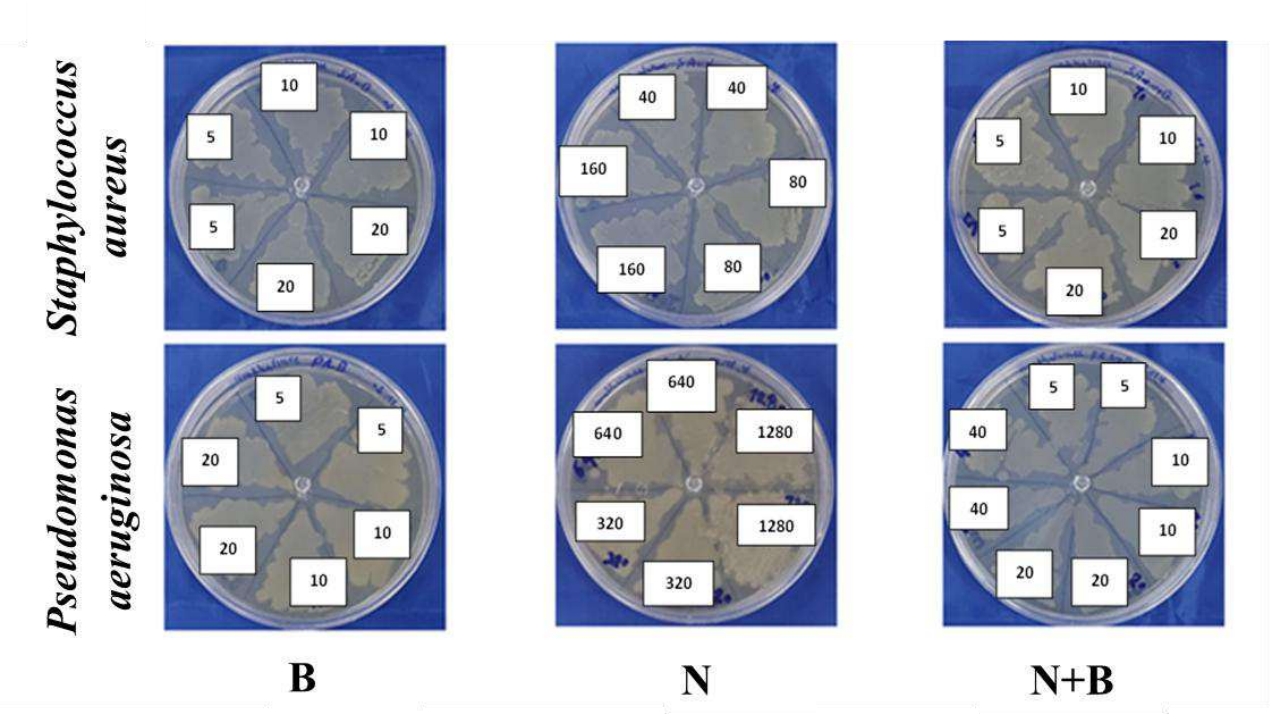



**Figure 12.** MBC results on *Staphylococcus aureus* and *Pseudomonas aeruginosa* at different groups of free BBR (B), blank SA NPs (N), and BBR-loaded SA NPs (N+B)

## 4. Discussion

In this study, sodium alginate nanoparticles encapsulating berberine were successfully prepared using the ionotropic gelation technique. Physicochemical analyses confirmed that BBR was efficiently loaded within the SA matrix, and the resulting NPs exhibited a narrow size distribution and a favorable surface charge. The drug-free SA NPs exhibited a near-neutral zeta potential, indicating limited electrostatic stability and a tendency toward aggregation. In contrast, BBR-loaded SA NPs showed a significantly more negative zeta potential (–21.4 mV), suggesting enhanced colloidal stability due to increased electrostatic repulsion between the

particles. This shift in surface charge can be attributed to the interaction of BBR with the SA matrix, likely through electrostatic interactions and hydrogen bonding, which alters the surface chemistry of the NPs. In addition to improved dispersion stability, the more negative zeta potential may influence biological interactions such as cellular uptake and protein adsorption (54). Here, we utilized honey to serve only as a processing stabilizer during nanoparticle fabrication, which was removed by repeated centrifugation and washing steps before subsequent analyses. The selection of honey was further supported by its natural and renewable origin, which makes it a potentially greener alternative to some conventional synthetic stabilizers. The use of biodegradable naturally derived materials may also help reduce concerns associated with the environmental persistence of chemical stabilizing agents.

EE and drug LC of the BBR-loaded NPs showed a highly efficient encapsulation process and a substantial proportion of drug content relative to the total NPs mass. However, the yield of BBR-loaded NPs was lower than that of SA NPs. The reduction in yield upon drug incorporation may be attributed to changes in particle formation dynamics, increased viscosity of the formulation, or partial loss of material during the encapsulation process. Despite the decrease, the yield remains within an acceptable range for nanoparticle-based drug delivery systems and reflects the successful integration of BBR into the carrier matrix (55).

BBR-containing SA NPs showed slow and sustained release, which is beneficial for maintaining effective drug levels over long periods. Such release behavior can reduce dosing frequency and limit related side effects. Many of the previously reported formulations on BBR-loaded polymer NPs exhibited relatively rapid BBR release profiles. For example, Taebpour et al. (27) developed and characterized PLGA-based polymeric NPs loaded with BBR to improve its delivery and anticancer activity. The NPs were synthesized using a double emulsion (W/O/W) method and were analyzed for their size, zeta potential, drug loading efficiency, and drug release. Their results showed a release of 61.46% and ~ 80% for 48 h in PBS, respectively, at 37 ° C and PH = 7.4, and at 42 ° C and PH = 5.2 from BBR-loaded PLGA NPs. Despite the relatively rapid release, enhanced cytotoxicity compared to free BBR was observed, suggesting improved therapeutic potential for breast cancer. Moreover, Ghaffarzadegan et al. (28) fabricated BBR-loaded poly lactic acid (PLA) NPs using coaxial electrospray to produce core-shell structures. This method enabled controlled encapsulation of BBR within the PLA polymer, resulting in NPs with uniform size and controlled drug release properties. The optimized formulation

demonstrated that 57% and 43% BBR release over 240 h, respectively in PBS with pH of 5.8 or 7.4 having the velocity of 100 rpm at 37 °C. Their formulation offered advantages for improving BBR's bioavailability and therapeutic efficacy. Furthermore, the burst BBR release reported in many existing studies on BBR-loaded SA-based NPs, often resulting in most of the drug diminution within a few hours, may impede the success of maximum therapeutic potential (29, 33, 36). Remarkably, the present study successfully engineered BBR-loaded SA NPs using calcium chloride that demonstrated a highly prolonged and controlled release profile, with only 10% of the encapsulated drug released over a 14-day period. The highly prolonged release profile can be attributed, at least in part, to $Ca^{2+}$-mediated ionic crosslinking of the SA chains, which likely produced a denser polymeric network and reduced the rate of water penetration and BBR diffusion from the NPs. In our previous study, the effect of crosslinker concentration on the particle size of SA NPs was systematically examined; therefore, the selected $CaCl_2$ level was retained in the present work to evaluate its performance in terms of sustained release and biological behavior (37). This substantial achievement underscores a superior ability to suppress the common *"burst effect"* observed in earlier delivery systems. By ensuring this sustained release, the formulation offers a significant advantage for applications requiring long-term therapeutic exposure, such as the treatment of chronic bone-related inflammatory diseases or sustained anticancer therapy. Moreover, this prolonged release capability minimizes the risk of toxicity associated with rapid drug accumulation while maximizing the pharmacological efficacy of BBR, thereby establishing a robust platform for future clinical translation. This was confirmed by the biocompatibility assessment of the synthesized NPs on normal osteoblastic cells. The observed MC3T3-E1 cell viability in all concentrations of free BBR, SA NPs, and BBR-loaded SA NPs was more than 70% at all time points. This high viability indicates that the normal cells tolerate nanoparticle or drug levels without significant stress and death.

In addition, the NPs promoted cellular differentiation, suggesting possible applications in tissue engineering and regenerative medicine. Our observation that 640 μg/mL of BBR-loaded SA NPs produced the strongest osteogenic responses (ALP concentration and Alizarin Red staining), is consistent with previous reports showing that BBR stimulates osteogenic differentiation. In a study, Xin et al. found that BBR enhanced osteogenic differentiation of human dental pulp stem cells via activation of EGFR-MAPK-Runx2 pathways, highlighting the molecular basis for

BBR-induced bone formation (56). The authors reported dose-response patterns for enhanced ALP activity and mineralization for BBR in dental pulp stem cell model, supporting the idea that an intermediate concentration can maximize osteoinduction, while higher concentrations may plateau or exert adverse effects. Furthermore, Minh et al. demonstrated that BBR-encapsulated NPs significantly increased ALP activity in MC3T3-E1 osteoblast cells relative to free BBR, indicating enhanced osteoblast differentiation and improved bioavailability of the nano formulated drug (57). Zhang et al. also showed that BBR treatment promoted osteogenic differentiation of mesenchymal stem cells (MSCs) by upregulating key osteogenic markers such as ALP, Osterix (OSX), collagen I, osteocalcin (OCN), and osteopontin (OPN), with involvement of the Wnt/β-catenin signaling pathway (58). The dose-dependent trend previously observed is consistent with the present findings, suggesting that controlled, lower concentrations of BBR within nanostructured systems may support osteogenic differentiation without inducing excessive cellular stress. Collectively, these results highlight the potential of BBR-loaded nanomaterials to modulate the bone microenvironment by simultaneously supporting differentiation-related processes and mitigating adverse biological responses.

The anti-inflammatory evaluation indicated that BBR-loaded SA NPs reduced the production of pro-inflammatory cytokines, with the most pronounced inhibitory effect observed at the lower concentrations. While the reduction in TNF-α levels reached statistical significance, the decrease in IL-6 secretion followed a downward trend, further reinforcing the biological relevance of the formulation. These findings suggest that the developed BBR-loaded SA NPs exert potent anti-inflammatory activity without inducing deleterious cytotoxic effects, particularly at lower doses, highlighting their potential for therapeutic applications in inflammatory tissue and bone pathologies. These observations align with previous studies; for instance, Guo et al. developed carrier-free co-assembly BBR- oleanolic acid (OA) NPs and demonstrated that BBR-loaded nanocarriers enhanced the anti-inflammatory efficacy of BBR by downregulating NO, TNF-α, IL-1β, and IL-6 (59). Similarly, Azadi et al. reported the concentration-dependent anti-inflammatory reduction of TNF-a, IL-1B, and MDA levels by BBR-loaded micelles, in a cerebral ischemia animal model (60), further validating the therapeutic promise of BBR-based nanocarriers in managing inflammatory response.

Our developed NPs formulation effectively inhibited cancer cell viability, particularly at 640 µg/mL concentration (MG63 viability of less than 50% at day 7), underscoring the potential of nanocarrier systems to enhance the therapeutic performance of natural bioactive compounds. A previous study has demonstrated that BBR-loaded nanocomposite scaffolds could effectively influence bone cancer (43). The developed BBR-loaded nano-hydroxyapatite/gelatin scaffolds showed that the released BBR had a cytotoxic effect on cancer cells both in early and late exposure, with a remarkable increase in the percentage of apoptotic MG63 cells in a dose-dependent manner. Furthermore, the authors revealed that all BBR-loaded scaffolds were able to significantly prevent cell migration and colony formation.

The BBR-loaded SA NPs were further examined for cellular uptake. These NPs were observed not only on the cell surface but also within the cytoplasmic region and, in some instances, in proximity to the nucleus, indicating efficient cellular internalization. This uptake pattern is consistent with previous reports (61-63). Alginate-based nanocarriers may enter cells mainly through energy-dependent endocytic pathways, facilitated by their nano-scale dimensions and favorable physicochemical properties. Although the BBR-loaded SA NPs exhibited a negative surface charge, which may reduce electrostatic interactions with the negatively charged cell membrane, their small size and the possible formation of a protein corona in biological environments can promote cellular interaction and uptake through endocytosis (64). It should be noted that in the presence of FBS-supplemented culture medium, a protein corona likely forms on the surface of the NPs (65). This layer can modify their effective surface charge and size, potentially modulating the electrostatic interactions with the cell membrane and facilitating the observed internalization. The intracellular localization of the nanoparticles suggests that the formulation successfully entered the cells and enabled intracellular delivery of BBR. Such effective uptake and intracellular distribution, particularly near the nucleus, may enhance the anti-inflammatory, antibacterial, and anticancer activities of BBR.

The antibacterial assays showed that BBR-loaded SA NPs produced stronger inhibitory effects against Gram-positive bacteria compared to Gram-negative bacteria. The superior activity of BBR-loaded SA NPs against Gram-positive bacteria may be attributed to their structural and electrochemical differences. Gram-positive bacteria lack an outer membrane, allowing improved nanoparticle penetration and BBR uptake, whereas the lipopolysaccharide-rich outer membrane

of Gram-negative species presents a strong permeability and electrostatic barrier. The moderately negative zeta potential (–21.4 mV) of the NPs may further limit interactions with the electronegative Gram-negative surface, while still permitting adhesion to the more accessible and structurally porous peptidoglycan of Gram-positive strains. Additionally, the inherent preference of BBR for Gram-positive targets and restricted drug entry/efflux phenomena in Gram-negative bacteria likely contribute to the observed activity trends. Here, our findings demonstrated slight differences in antibacterial properties among free BBR, and drug-free and drug loaded NPs. This is in contrast with previous research. Nguyen et al. reported that BBR NPs prepared via anti-solvent precipitation exhibited markedly stronger antibacterial activity against both *Escherichia coli* O157:H7 and methicillin-resistant *Staphylococcus aureus* (MRSA) than free BBR, as evidenced by lower MIC and MBC values and pronounced bacterial cell wall disruption observed by electron microscopy (66). Similarly, Sadeghi et al. showed that BBR conjugated with gold NPs displayed superior antibacterial and anti-biofilm activity against MRSA compared to free BBR, which was attributed to enhanced bacterial membrane interaction and increased reactive oxygen species generation (67). One possible reason for this discrepancy may be related to the sustained and slow drug release rate of the developed NPs, with only approximately 10% of BBR released over 14 days. Unlike the formulations designed for rapid drug liberation, which can induce an immediate and pronounced antibacterial effect, our engineered system provides a controlled and prolonged release, resulting in lower initial extracellular drug concentrations. Although, this may attenuate short-term antibacterial potency in standard MIC/MBC assays, it offers several important advantages. This includes reduced burst-related toxicity, improved drug stability, and maintenance of sub-therapeutic yet biologically active concentrations over an extended period. This drug release behavior is particularly desirable for applications requiring long-term inflammation modulation, tissue regeneration, or anticancer activity, where sustained exposure rather than acute dosing is critical. Furthermore, prolonged release may aid in minimizing the development of bacterial resistance and enhance therapeutic efficacy in chronic or localized treatment settings, such as those integrated into scaffold- or hydrogel-based delivery systems for applications like osteomyelitis or in dentistry. Mechanistically, the observed slow-release profile is attributable to the combined effects of berberine's chemistry and the ionically cross-linked structure of calcium-alginate. Berberine is a quaternary isoquinoline

alkaloid that exists as a permanently cationic (iminium/quaternary ammonium) species at physiological pH; this cationic character promotes electrostatic association with deprotonated alginate carboxylates. Concurrently, Ca2+ ions form "egg-box" junctions between guluronate blocks, increasing crosslink density and mesh tortuosity of the gel network (68), which reduces effective diffusivity and contributes to drug retention. These electrostatic associations, together with reduced pore connectivity and possible hydrophobic/π-stacking interactions of the planar berberine molecule, rationalize the reduced burst release and prolonged release kinetics observed.

Taken together, the pharmacodynamic profile (biological activity) and the pharmacokinetic behavior (slow, sustained release) were mutually consistent. Specifically, the sustained intracellular delivery and prolonged extracellular exposure at the 640 μg/mL provided a favorable exposure window for bone cell viability, osteogenic activity, anti-inflammatory effect, and anti-cancer activity, with slight and moderate antibacterial effect, respectively, against *Pseudomonas aeruginosa* and *Staphylococcus aureus*. This formulation avoided the diminishing returns or toxicity, which is sometimes seen at higher concentrations. These mechanistic and comparative considerations reinforce the interpretation that 640 μg/mL represents an optimal balance between efficacy and controlled release of the BBR-loaded SA NPs formulation.

## 5. Conclusion

This study demonstrated that sodium alginate nanoparticles prepared via ionotropic gelation could offer an effective and versatile delivery system for berberine. By enhancing the compound’s stability, and controlled release, the nanoparticle formulation revealed non-toxicity to normal bone cells, anti-inflammatory activity, differentiation-promoting toward osteoblasts, cellular uptake, and anti-cancer activity, with slight and moderate antibacterial effect, respectively, against *Pseudomonas aeruginosa* and *Staphylococcus aureus*. These findings underscore the value of SA nano-carriers in biomedical use. Nevertheless, further in vivo studies and eventual clinical investigations are needed to confirm their suitability for advanced biomedical and pharmaceutical applications.

**Abbreviation list:**

| | |
|---|---|
| Berberine | BBR |
| Sodium alginate | SA |
| dynamic light scattering | DLS |
| Fourier transform infrared spectroscopy | FTIR |
| field emission scanning electron microscopy | FE-SEM |
| United States | USA |
| Nanoparticles | NPs |
| Dulbecco's Modified Eagle Medium | DMEM |
| Fetal bovine serum | FBS |
| Alkaline phosphatase assay | ALP |
| Minimum inhibition concentration | MIC |
| Minimum Bactericidal Concentration | MBC |
| Entrapment Efficiency | EE |
| the loading capacity of the drug | LC |
| Analysis of variance | ANOVA |
| Design of Experiments | DOE |
| Osteoblast precursor cell line derived from Mus musculus | MC3T3-E1 |
| Human osteosarcoma cell line | MG-63 |
| Staphylococcus aureus strain | SA |
| NPs without BBR | N |
| NPs with BBR | N+B |

**Ethical Approval and accordance**

All assays were confirmed by the Ethics Committee of the Semnan Medical University Faculty of Medicine, Iran with IR.SEMUMS.REC.1401.220 certificate number.

**Declaration of conflicting interests**

The author(s) declared no potential conflicts of interest concerning the research, authorship, and/or publication of this article.

**Consent to publish declaration**

Not applicable

**Clinical trial registration**

Not applicable

**Availability of data and material**

The datasets used and analyzed during the current study are available from the corresponding or first author on reasonable request.

**Funding**

This study was supported by a grant from Semnan University of Medical Sciences (Grant No.2136).

**Authors' contributions**

- **Mohadeseh Arabhalvaei** conducted experiments, and wrote the first draft of the manuscript (mohadeseh.6790@gmail.com)
- **Marjan Bahraminasab** designed the experiments, conducted data analyses, prepared figures, supervised the project, wrote the first draft and edited the final the manuscript (m.bahraminasab@yahoo.com)
- **Zahra Nazemi** Consultancy, review and editing (nazemi.z@gmail.com)
- **Samaneh Arab** Consultancy, review and editing (samaneh.arab@gmail.com)
- **Akram Alizadeh** Consultancy, review and editing (alizadehbio@gmail.com)
- **Mohammad Sadegh Nourbakhsh** Consultancy, review and editing (s_nourbakhsh@semnan.ac.ir)

– All authors discussed the results of experiments, edited and approved the final version of the manuscript.


## Acknowledgments

The authors would like to thank Semnan University of medical sciences for funding this research.


## Consent to participate

Not applicable.

## References:


1. Alolga RN, Fan Y, Chen Z, Liu L-W, Zhao Y-J, Li J, et al. Significant pharmacokinetic differences of berberine are attributable to variations in gut microbiota between Africans and Chinese. Scientific reports. 2016;6(1):27671.
2. Gaba S, Saini A, Singh G, Monga V. An insight into the medicinal attributes of berberine derivatives: A review. Bioorg Med Chem. 2021;38:116143.
3. Chen L, Tian M, Yang J, Wu Z. Berberine-Encapsulated Poly(lactic-co-glycolic acid)-Hydroxyapatite (PLGA/HA) Microspheres Synergistically Promote Bone Regeneration with DOPA-IGF-1 via the IGF-1R/PI3K/AKT/mTOR Pathway. Int J Mol Sci. 2023;24(20).
4. Yang B, Sun H, Xu X, Zhong H, Wu Y, Wang J. YAP1 inhibits the induction of TNF-α-stimulated bone-resorbing mediators by suppressing the NF-κB signaling pathway in MC3T3-E1 cells. J Cell Physiol. 2020;235(5):4698-708.
5. Och A, Podgórski R, Nowak R. Biological Activity of Berberine-A Summary Update. Toxins (Basel). 2020;12(11).
6. Almatroodi SA, Alsahli MA, Rahmani AH. Berberine: An Important Emphasis on Its Anticancer Effects through Modulation of Various Cell Signaling Pathways. Molecules. 2022;27(18).
7. Zhang C, Sheng J, Li G, Zhao L, Wang Y, Yang W, et al. Effects of Berberine and Its Derivatives on Cancer: A Systems Pharmacology Review. Front Pharmacol. 2019;10:1461.
8. Xiong RG, Huang SY, Wu SX, Zhou DD, Yang ZJ, Saimaiti A, et al. Anticancer Effects and Mechanisms of Berberine from Medicinal Herbs: An Update Review. Molecules. 2022;27(14).
9. S Khajavi MB, S Arab, A Talebi, P Kokhaei, H Abdoos. Design and synthesis of berberine loaded nano-hydroxyapatite/gelatin scaffold for bone cancer treatment. New Journal of Chemistry. 2024.
10. Ehterami A, Abbaszadeh-Goudarzi G, Haghi-Daredeh S, Niyakan M, Alizadeh M, JafariSani M, et al. Bone tissue engineering using 3-D polycaprolactone/gelatin nanofibrous scaffold containing berberine: In vivo and in vitro study. Polymers for Advanced Technologies. 2022;33(2):672-81.
11. Cui Y, Xie J, Cai L, Zhang D, Sun J, Zhou X. Berberine regulates bone metabolism in apical periodontitis by remodelling the extracellular matrix. Oral diseases. 2023;29(3):1184-96.
12. Gaba S, Saini A, Singh G, Monga V. An insight into the medicinal attributes of berberine derivatives: A review. Bioorganic & Medicinal Chemistry. 2021;38:116143.
13. Ai X, Yu P, Peng L, Luo L, Liu J, Li S, et al. Berberine: A Review of its Pharmacokinetics Properties and Therapeutic Potentials in Diverse Vascular Diseases. Front Pharmacol. 2021;12:762654.

14. Ye M, Fu S, Pi R, He F. Neuropharmacological and pharmacokinetic properties of berberine: a review of recent research. Journal of Pharmacy and Pharmacology. 2009;61(7):831-7.
15. Islam S, Ahmed MMS, Islam MA, Hossain N, Chowdhury MA. Advances in nanoparticles in targeted drug delivery–A review. Results in Surfaces and Interfaces. 2025;19:100529.
16. Afzal O, Altamimi AS, Nadeem MS, Alzarea SI, Almalki WH, Tariq A, et al. Nanoparticles in drug delivery: from history to therapeutic applications. Nanomaterials. 2022;12(24):4494.
17. Khatib Zadeh Z, Arab S, Kazemi S, Arabhalvaei M, Afraz ES, Bahraminasab M. In vitro anticancer effect of epigallocatechin gallate nano-emulsion on head and neck cancers. Clinical and Translational Oncology. 2025;27(9):3745-62.
18. Wang X, Fu L, Cheng W, Chen J, Zhang H, Zhu H, et al. Oral administration of Huanglian-Houpo herbal nanoemulsion loading multiple phytochemicals for ulcerative colitis therapy in mice. Drug Delivery. 2023;30(1):2204207.
19. Nikezić AVV, Bondžić AM, Vasić VM. Drug delivery systems based on nanoparticles and related nanostructures. Eur J Pharm Sci. 2020;151:105412.
20. Cheng H, Chawla A, Yang Y, Li Y, Zhang J, Jang HL, et al. Development of nanomaterials for bone-targeted drug delivery. Drug Discov Today. 2017;22(9):1336-50.
21. Begines B, Ortiz T, Pérez-Aranda M, Martínez G, Merinero M, Argüelles-Arias F, et al. Polymeric Nanoparticles for Drug Delivery: Recent Developments and Future Prospects. Nanomaterials (Basel). 2020;10(7).
22. Cui P-F, Zhuang W-R, Hu X, Xing L, Yu R-Y, Qiao J-B, et al. A new strategy for hydrophobic drug delivery using a hydrophilic polymer equipped with stacking units. Chemical Communications. 2018;54(59):8218-21.
23. Kumari A, Yadav S, Yadav S. Biodegradable polymeric nanoparticles based drug delivery systems. Colloids and surfaces B, Biointerfaces. 2009;75:1-18.
24. Wang Y, Wen B, Yu H, Ding D, Zhang J, Zhang Y, et al. Berberine Hydrochloride-Loaded Chitosan Nanoparticles Effectively Targets and Suppresses Human Nasopharyngeal Carcinoma. J Biomed Nanotechnol. 2018;14(8):1486-95.
25. Li Z, Geng Y-N, Jiang J-D, Kong W-J. Antioxidant and Anti-Inflammatory Activities of Berberine in the Treatment of Diabetes Mellitus. Evidence-Based Complementary and Alternative Medicine. 2014;2014(1):289264.
26. Mirhadi E, Rezaee M, Malaekeh-Nikouei B. Nano strategies for berberine delivery, a natural alkaloid of Berberis. Biomedicine & Pharmacotherapy. 2018;104:465-73.
27. Taebpour M, Arasteh F, Akhlaghi M, Haghirosadat BF, Oroojalian F, Tofighi D. Fabrication and characterization of PLGA polymeric nanoparticles containing Berberine and its cytotoxicity on breast cancer cell (MCF-7). Nanomedicine Research Journal. 2021;6(4):396-408.
28. Ghaffarzadegan R, Khoee S, Rezazadeh S. Fabrication, characterization and optimization of berberine-loaded PLA nanoparticles using coaxial electrospray for sustained drug release. Daru. 2020;28(1):237-52.
29. Kohli K, Mujtaba A, Malik R, Amin S, Alam MS, Ali A, et al. Development of Natural Polysaccharide-Based Nanoparticles of Berberine to Enhance Oral Bioavailability: Formulation, Optimization, Ex Vivo, and In Vivo Assessment. Polymers (Basel). 2021;13(21).
30. Tønnesen HH, Karlsen J. Alginate in drug delivery systems. Drug development and industrial pharmacy. 2002;28(6):621-30.
31. Bahraminasab M, Janmohammadi M, Arab S, Talebi A, Nooshabadi VT, Koohsarian P, et al. Bone Scaffolds: An Incorporation of Biomaterials, Cells, and Biofactors. ACS Biomater Sci Eng. 2021;7(12):5397-431.
32. Fernando IPS, Kim D, Nah J-W, Jeon Y-J. Advances in functionalizing fucoidans and alginates (bio)polymers by structural modifications: A review. Chemical Engineering Journal. 2019;355:33-48.

33. Mehra M, Sheorain, J., Bakshi, J., Grewal, S., Dhingra, D., Bernela, M., & Kumari, S. . Sodium alginate polymer nanoformulation as promising carrier for berberine delivery: synthesis, morphology and in-vitro evaluation. . Carbohydrate Polymer Technologies and Applications, 7, 100408. 2024.
34. Hasannejad F, Arab S, Farahmand L, Darvishi B, Bahraminasab M. Design and optimization of thermosensitive injectable alginate-based hydrogels: potential for loading therapeutic compounds2023.
35. Bahraminasab M, Asgharzade S, Doostmohamadi A, Satari A, Hasannejad F, Arab S. Development of a hydrogel-based three-dimensional (3D) glioblastoma cell lines culture as a model system for CD73 inhibitor response study. Biomed Eng Online. 2024;23(1):127.
36. - Kumar V, Kumar, P., & Sharma, S. . Application of box-behnken experimental design in process parameter optimization for production of berberine HCl loaded chitosan coated sodium alginate nanoparticles. . Research Journal of Pharmacy and Technology, . 2023;16, ((3)):1139-46.
37. Rajabzadeh F, Arabhalvaei M, Arab S, Afraz ES, Bahraminasab M. Exploring the anticancer potential of epigallocatechin gallate-loaded sodium alginate nanoparticles: impact of size variation on head and neck cancer cells. Clinical and Translational Oncology. 2026:1-19.
38. Geetha P, S L, Pillai S, B D, Kumar KS, Koshy M. Green Synthesis and Characterization of Alginate Nanoparticles and its Role as a Biosorbent for Cr(VI) Ions. Journal of Molecular Structure. 2015;1105.
39. Tao K, Xiao D, Weng J, Xiong A, Kang B, Zeng H. Berberine promotes bone marrow-derived mesenchymal stem cells osteogenic differentiation via canonical Wnt/β-catenin signaling pathway. Toxicology letters. 2016;240(1):68-80.
40. Chen L, Tian M, Yang J, Wu Z. Berberine-encapsulated poly (lactic-co-glycolic acid)–hydroxyapatite (PLGA/HA) microspheres synergistically promote bone regeneration with DOPA-IGF-1 via the IGF-1R/PI3K/AKT/mTOR pathway. International Journal of Molecular Sciences. 2023;24(20):15403.
41. Li M, Qin Z, Yu Q, Huang Z, Cheng J, Zhong L, et al. Anti-inflammatory activation of phellodendri chinensis cortex is mediated by berberine erythrocytes self-assembly targeted delivery system. Drug Design, Development and Therapy. 2022:4365-83.
42. Xu R, He H, Deng H, Dong Y, Wu X, Xia Z, et al. Study of conductive nerve conduits for anti-inflammatory and antioxidant effects. RSC advances. 2025;15(18):14136-51.
43. Khajavi S, Bahraminasab M, Arab S, Talebi A, Kokhaei P, Abdoos H. Design and synthesis of berberine loaded nano-hydroxyapatite/gelatin scaffold for bone cancer treatment. New Journal of Chemistry. 2024;48(15):6977-96.
44. Zhang C, Li Z, Pan Q, Fan L, Pan T, Zhu F, et al. Berberine at sub-inhibitory concentration inhibits biofilm dispersal in Staphylococcus aureus. Microbiology (Reading). 2022;168(9).
45. Mehra M, Sheorain J, Bakshi J, Thakur R, Grewal S, Dhingra D, et al. Synthesis and evaluation of berberine loaded chitosan nanocarrier for enhanced in-vitro antioxidant and anti-inflammatory potential. Carbohydrate Polymer Technologies and Applications. 2024;7:100474.
46. Liang S, Wang L. A natural antibacterial-antioxidant film from soy protein isolate incorporated with cortex phellodendron extract. Polymers. 2018;10(1):71.
47. Bashmakova N, Kutovyy S, Zhurakivsky R, Hovorun D, Yashchuk V. Vibrational spectra of berberine and their interpretation by means of DFT quantum-mechanical calculations. arXiv preprint arXiv:11034290. 2011.
48. Jia J, Zhang K, Zhou X, Zhou D, Ge F. Precise dissolution control and bioavailability evaluation for insoluble drug berberine via a polymeric particle prepared using supercritical CO2. Polymers. 2018;10(11):1198.
49. Saikia S, Khanam SA, Kandali P, Guha AK, Bania KK. Photodegradation of berberine hydrochloride at the interface of 1D–2D nanohybrid of nickel ferrite supported on reduced graphene oxidhttps://doi.org/10.1039/d4su00638k. RSC Sustainability. 2024;3(1):510-25.

50. Belattmania Z, Kaidi S, El Atouani S, Katif C, Bentiss F, Jama C, et al. Isolation and FTIR-ATR and 1H NMR Characterization of Alginates from the Main Alginophyte Species of the Atlantic Coast of Morocco. Molecules. 2020;25(18):4335.
51. Shankar S, Kasapis S, Rhim JW. Alginate-based nanocomposite films reinforced with halloysite nanotubes functionalized by alkali treatment and zinc oxide nanoparticles. Int J Biol Macromol. 2018;118(Pt B):1824-32.
52. Kohli K, Mujtaba A, Malik R, Amin S, Alam MS, Ali A, et al. Development of Natural Polysaccharide–Based Nanoparticles of Berberine to Enhance Oral Bioavailability: Formulation, Optimization, Ex Vivo, and In Vivo Assessment. Polymers. 2021;13(21):3833.
53. Havrdova M, Polakova K, Skopalik J, Vujtek M, Mokdad A, Homolkova M, et al. Field emission scanning electron microscopy (FE-SEM) as an approach for nanoparticle detection inside cells. Micron. 2014;67:149-54.
54. Patil S, Sandberg A, Heckert E, Self W, Seal S. Protein adsorption and cellular uptake of cerium oxide nanoparticles as a function of zeta potential. Biomaterials. 2007;28(31):4600-7.
55. Abdelmonem R, Ayman M, lofty SE, Ezzat Y, Nabeah Jm, Mohamed H, et al. Advancing Nanoparticle Production: Scaling Up Techniques, Challenges, and Future Perspectives in Pharmaceutical Applications. Journal of Pharmaceutical Sciences and Drug Manufacturing-Misr University for Science and Technology. 2025;2(2):26-39.
56. Xin BC, Wu QS, Jin S, Luo AH, Sun DG, Wang F. Berberine Promotes Osteogenic Differentiation of Human Dental Pulp Stem Cells Through Activating EGFR-MAPK-Runx2 Pathways. Pathology oncology research : POR. 2020;26(3):1677-85.
57. 1.Minh NTH TAT, Thuy Duong LT, Viet Linh N, Phuong NTM. [Internet]. 2021 May 24 [cited Feb. 9]. Available from: https://vjs.ac.vn/vjbt/article/view/15311 Berberine encapsulated nanoparticles stimulate osteoblast differentiation in vitro. . Vietnam J Biotechnol 2026 ;18(4):633-41.
58. Zhang R, Yang J, Wu J, Xiao L, Miao L, Qi X, et al. Berberine promotes osteogenic differentiation of mesenchymal stem cells with therapeutic potential in periodontal regeneration. Eur J Pharmacol. 2019;851:144-50.
59. Guo G, Zhang Z, Xia X, He Z, Jiang N, Liu X, et al. Berberine-oleanolic acid self-assembled nanoparticles: Enhanced stability, cellular uptake, and anti-inflammatory activity. Journal of Molecular Structure. 2025:144577.
60. Azadi R, Mousavi SE, Kazemi NM, Yousefi-Manesh H, Rezayat SM, Jaafari MR. Anti-inflammatory efficacy of Berberine Nanomicelle for improvement of cerebral ischemia: Formulation, characterization and evaluation in bilateral common carotid artery occlusion rat model. BMC Pharmacology and Toxicology. 2021;22(1):54.
61. Zhang P, Zhao S, Yu Y, Wang H, Yang Y, Liu C. Biocompatibility Profile and In Vitro Cellular Uptake of Self-assembled Alginate Nanoparticles. Molecules. 2019;24(3):555.
62. Salatin S, Yari Khosroushahi A. Overviews on the cellular uptake mechanism of polysaccharide colloidal nanoparticles. Journal of cellular and molecular medicine. 2017;21(9):1668-86.
63. Zhu X, Su M, Tang S, Wang L, Liang X, Meng F, et al. Synthesis of thiolated chitosan and preparation nanoparticles with sodium alginate for ocular drug delivery. Molecular vision. 2012;18:1973.
64. de Almeida MS, Susnik E, Drasler B, Taladriz-Blanco P, Petri-Fink A, Rothen-Rutishauser B. Understanding nanoparticle endocytosis to improve targeting strategies in nanomedicine. Chemical society reviews. 2021;50(9):5397-434.
65. Shannahan JH, Brown JM, Chen R, Ke PC, Lai X, Mitra S, et al. Comparison of nanotube–protein corona composition in cell culture media. Small. 2013;9(12):2171-81.
66. Nguyen TX HL, Liu L, El-Hady DA, Chen Y, Huang Q. Antibacterial activity of berberine nanoparticles against Escherichia coli O157:H7 and methicillin-resistant Staphylococcus aureus. Int J Nanomedicine. 2022;17: 5401-5415.

67. Sadeghi S, Agharazi F, Hosseinzadeh SA, Mashayekhi M, Saffari Z, Shafiei M, et al. Gold nanoparticle conjugation enhances berberine's antibacterial activity against methicillin-resistant Staphylococcus aureus (MRSA). Talanta. 2024;268(Pt 1):125358.
68. Wang Y, Zhao Y, He J, Sun C, Lu W, Zhang Y, et al. Doubling growth of egg-box structure during Calcium-mediated molecular assembly of alginate. Journal of colloid and interface science. 2023;634:747-56.

## Supplementary Files

This is a list of supplementary files associated with this preprint. Click to download.

- GAjpg.jpg